united nations
educational, scientific
and cultural
organization

international atomic
energy agency

the
abdus salam
international centre for theoretical physics

SMR 1216 - 2

**Joint INFM - the Abdus Salam ICTP School on
"Magnetic Properties of Condensed Matter Investigated by Neutron Scattering and Synchrotron Radiation Techniques"**

1 - 11 February 2000

MAGNETIC NEUTRON SCATTERING

Albert FURRER
Laboratory for Neutron Scattering
Swiss Federal Institute of Technology Zurich & Paul Scherrer Institute
CH-5232 Villigen PSI, Switzerland

School on

"Magnetic Properties of Condensed Matter Investigated by

Neutron Scattering and Synchrotron Radiation Techniques"

1-11 February 2000, Trieste, Italy

Magnetic Neutron Scattering

Albert Furrer

Laboratory for Neutron Scattering

Swiss Federal Institute of Technology Zurich & Paul Scherrer Institute

CH-5232 Villigen PSI

albert.furrer@psi.ch

Contents:

1. Neutron Sources

(This Chapter on "Neutron Sources" is an exerpt from a review article by Bauer [1]). There is an almost unlimited range of research and applications in science in which neutron scattering plays an essential role in solving difficult and important problems. Unfortunately, suitable neutrons are not readily available. Although about half of our world is made up of neutrons, they are tightly bound deep inside the atomic nucleus and quite difficult to set free. Facilities that accomplish this task in a manner useful for scientific and technological applications are called neutron sources. The energies of free neutrons span many orders of magnitude. Table 1.1 gives a summary of terms commonly used to characterise different neutron energy regimes.

Table 1.1: Approximate limits of neutron energy regimes classified by names.

Energy range	Classification		Energy Range for
	Nuclear Physics	Neutron Scattering	Neutron Scattering
		ultra cold	< 0.1 meV
		very cold	0.1 ÷ 0.5 meV
< 1 keV	slow	cold	0.5 ÷ 5 meV
		thermal	5 ÷ 100 meV
		epithermal or hot	0.1 ÷ 1 eV
		resonant	1 ÷ 100 eV
1 keV ÷ 0.5 MeV	intermediate		
0.5 ÷ 10 MeV	fast		
10 ÷ 50 MeV	very fast		
50 MeV ÷ 10 GeV	high energy or ultra fast		
> 10 GeV	relativistic		

For all neutron sources we are dealing with nuclear reactions. Some nuclear reactions with a practical potential are listed in Table 1.2. Since the goal must be to release as many neutrons as possible in as small a volume as possible to achieve a high luminosity, the heat deposition going along with the neutron release is an important

feature and has been included in Table 1.2. In fact, cooling problems are a limiting factor in practically all neutron source designs. The two most commonly used reactions are thermal nuclear fission in ^{235}U and spallation by protons in the energy range around 1 GeV. We will restrict ourselves to these reactions.

Table 1.2: Neutron yields and deposited heat for some neutron producing reactions.

Reaction and Energy/Event		Yield [n/event]	Deposited heat [MeV/n]
T(d,n):	0.2 MeV	8×10^{-5} n/d	2500
W(e,n):	35 MeV	1.7×10^{-2} n/e	2000
^{9}Be(d,n):	15 MeV	1.2×10^{-2} n/d	1200
^{235}U(n,f) fission		~ 1 n/fission	200
(T,d) fusion		~ 1 n/fusion	3
Pb spallation:	1 GeV	~ 20 n/p	23
^{238}U spallation:	1 GeV	~ 40 n/p	50

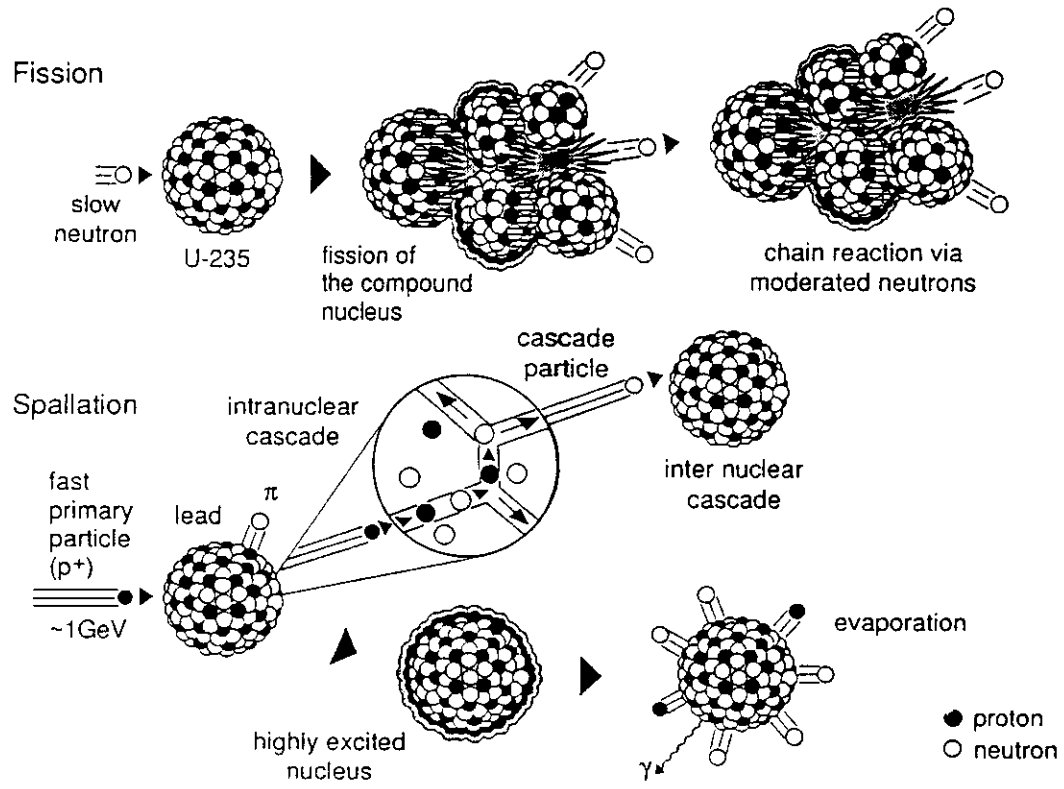

Fig. 1.1: Schematic representation of fission and spallation.

Fission of the uranium isotope 235 by slow neutron capture has been the most frequently used reaction in neutron sources up to the present. The reaction can be made self-sustaining because it is exothermal and releases more neutrons per fission process than are needed to initiate the process. If a slow neutron is captured by a fissionable nucleus, the resulting deformation can cause the nucleus to break into two fragments (see Fig. 1.1). Very often a neutron is released directly during this process, but mostly the neutrons "evaporate" from the fragments. This is a very important feature, because a small fraction of these evaporation neutrons are released with a time delay of the order of seconds (up to minutes) and thus enable a critical arrangement to be run in a controlled fashion.. The spectral distribution of the fission neutrons can be well described by a Maxwellian

$$n(E) = \frac{2}{\pi^{1/2} \cdot E_T^{3/2}} \sqrt{E} \cdot \exp\left\{-\frac{E}{E_T}\right\} \qquad (1.1)$$

with a characteristic energy E_T=1.29 MeV. Fission reactors produce a **continuous** flux of neutrons.

The term **"spallation"** is applied to a sequence of events that take place, if target nuclei are bombarded with particles (e.g., protons) of a de Broglie wavelength $\lambda = \sqrt{h^2/2mE}$ which is shorter than the linear dimension of the nucleus. In this case collisions can take place with individual nuclides inside the nucleus and large amounts of energy are transferred to the nuclides which, in turn, can hit other nuclides in the same nucleus. The net effect of this intra-nuclear cascade is twofold (see Fig. 1.1): Firstly, energy is more or less evenly distributed over the nucleus leaving it in a highly excited state; secondly, energetic particles may leave the nucleus and carry the cascade on to the other nuclei (inter-nuclear cascade) or escape from the target. The excited nucleus left behind will start to evaporate neutrons (and to a lesser extent protons). The low-energy part of the spectrum of these evaporation neutrons is quite similar to the one resulting from fission (eq. 1.1), but as a consequence of the neutron escape during the intra-nuclear cascade the spectrum extends to energies up to that of the incident particles (i.e., up to 1 GeV). The release of spallation neutrons takes place within less than 10^{-15} s

after the nucleus was hit, so that the time distribution of spallation neutrons is exclusively determined by the time distribution of the driving particle pulse, i.e., spallation sources deliver a **pulsed** flux of neutrons.

The energy spectrum of neutrons released from the neutron source is in the MeV range, whereas meV neutrons are required for scattering experiments. Therefore an energy shift of several orders of magnitude is necessary, which is accomplished by collisions with the atoms of a **moderator** substance. The goal in the layout of a moderator is to create the highest possible flux of moderated neutrons either in the shortest possible time (pulsed neutron sources) or in the largest possible volume (steady state neutron sources). It is therefore desirable that as many collisions as possible occur in the shortest possible time. This can be achieved by using moderators made of light atoms such as H_2O and D_2O. The time for slowing down the neutrons is of the order of 10^{-6} s after which the neutrons are in thermal equilibrium with the moderator according to the Maxwellian distribution defined by eq. (1.1). Moderators are usually kept at room temperature, and this is the reason why the corresponding neutrons are called **thermal neutrons**, with a maximum peak flux around the neutron wavelength $\lambda \approx 1$ Å ($E \approx 80$ meV). The Maxwellian energy spectrum of the neutrons can be shifted by inserting either a cold source (e.g., a vessel containing D_2 at $T \approx 20$ K) or a hot source (e.g., a graphite bloc heated to $T \approx 2000$ K) into the moderator.

2. Basic Properties of the Neutron

The most relevant, unique character of thermal neutrons, which can hardly be matched by any other experimental technique, can be summarized as follows:

- The neutron interacts with the atomic nucleus, and not with the electrons as x-rays do. This has important consequences: The response of neutrons from light atoms (e.g., hydrogen, oxygen) is much higher than for x-rays; neutrons can easily distinguish atoms of comparable atomic number; and finally, neutrons easily distinguish isotopes which allows, e.g., by deuteration of specific parts of

macromolecules (or biological substances) to focus on specific aspects of their atomic arrangement.

- For the same wavelength as hard x-rays the neutron energy is much lower and comparable to the energy of elementary excitations in matter. Therefore, neutrons do not only allow the determination of the "static average" chemical structure, but also the investigation of the dynamic properties of atomic arrangements which are directly related to the physical properties of materials.
- By virtue of its neutrality the neutron is rather weakly interacting with matter which means that there is almost no radiation damage to living biological objects under study. Also, the rather weak interaction with matter results in a large penetration depth and therefore the bulk properties of matter can be studied. This is also important for the investigation of materials under extreme conditions such as very low and very high temperatures, high pressures, high magnetic and electric fields, or several of these together; in such cases the studied sample is always surrounded by numerous shields which make the use of x-rays difficult.
- The neutron carries a magnetic moment which makes it an excellent probe for the determination of the static and dynamical magnetic properties of matter (magnetic ordering phenomena, magnetic excitations, spin fluctuations).

It is exactly this latter point which forms the basis of the work described in the present chapter.

The kinetic energy of a thermal neutron with velocity **v** is given by

$$E = \frac{mv^2}{2}, \tag{2.1}$$

where $m=1.675\cdot10^{-24}$ g is the mass of the neutron. The de Broglie wavelength λ of the neutron is defined by

$$\lambda = \frac{h}{mv}, \tag{2.2}$$

where h=6.626·10^{-27} erg·s is the Planck constant. The wave vector **k** of the neutron has the magnitude

$$k = \frac{2\pi}{\lambda} , \tag{2.3}$$

its direction being that of **v**. Eqs. (2.1)-(2.3) define the momentum **p** and the energy E of the neutron:

$$\mathbf{p} = \hbar\mathbf{k} , \tag{2.4}$$

$$E = \frac{\hbar^2 k^2}{2m} , \tag{2.5}$$

with $\hbar = h/2\pi$. It is conventional to say that a neutron with energy E corresponds to a temperature T:

$$E = k_B T , \tag{2.6}$$

where k_B=1.381·10^{-16} erg·K^{-1} is the Boltzmann constant. Combining eqs. (2.1)-(2.6) yields

$$E = \frac{h^2}{2m\lambda^2} = \frac{\hbar^2 k^2}{2m} = \frac{mv^2}{2} = k_B T . \tag{2.7}$$

By inserting the values of the elementary constants we arrive at the following relations between the energy, wave length, wave vector, velocity, and temperature for thermal neutrons:

$$E = 81.81 \frac{1}{\lambda^2} = 2.072\ k^2 = 5.227\ v^2 = 0.08617\ T , \tag{2.8}$$

where the units are meV for E, Å for λ, $Å^{-1}$ for k, km/s for v, and K (Kelvin) for T. In neutron scattering the energies are usually quoted in meV. Another energy unit frequently used is terahertz (THz), and other spectroscopic techniques often use wave numbers in units of cm^{-1}. We then have

$$1 \text{ meV} \equiv 0.242 \text{ THz} \equiv 8.07 \text{ cm}^{-1} \equiv 11.6 \text{ K} \equiv 17.3 \text{ T} , \tag{2.9}$$

where the conversions to temperature (K) and magnetic field (T=Tesla) are included for completeness.

3. Instrumental Aspects

The principal aim of a neutron scattering experiment is the determination of the probability that a neutron which is incident on the sample with wave vector **k** is scattered into the state with wave vector **k'**. The intensity of the scattered neutrons is thus measured as a function of the momentum transfer

$$\hbar\mathbf{Q} = \hbar(\mathbf{k} - \mathbf{k}') , \tag{3.1}$$

where **Q** is known as the scattering vector, and the corresponding energy transfer is given by

$$\hbar\omega = \frac{\hbar^2}{2m}(k^2 - k'^2) . \tag{3.2}$$

Eqs. (3.1) and (3.2) describe the momentum and energy conservation of the neutron scattering process, respectively. The momentum conservation is schematically sketched in Fig. 3.1. For k=k' we have from eq. (3.2) $\hbar\omega = 0$, i.e., elastic scattering. Fig. 3.1(a) shows the particular situation

$$\mathbf{Q} = \mathbf{k} - \mathbf{k}' = \tau \,, \tag{3.3}$$

which is just the condition known as Bragg's law (coherent elastic scattering). If **Q** does not coincide with a reciprocal lattice vector τ, we have incoherent elastic scattering. For inelastic scattering (b) the scattering vector can be decomposed according to $\mathbf{Q}=\tau+\mathbf{q}$, where **q** is the wave vector of an elementary excitation to be specified. Neutron scattering turns out to be the only experimental technique which is able to measure the dispersion relation $\hbar\omega(\mathbf{q})$ at any predetermined point in reciprocal space.

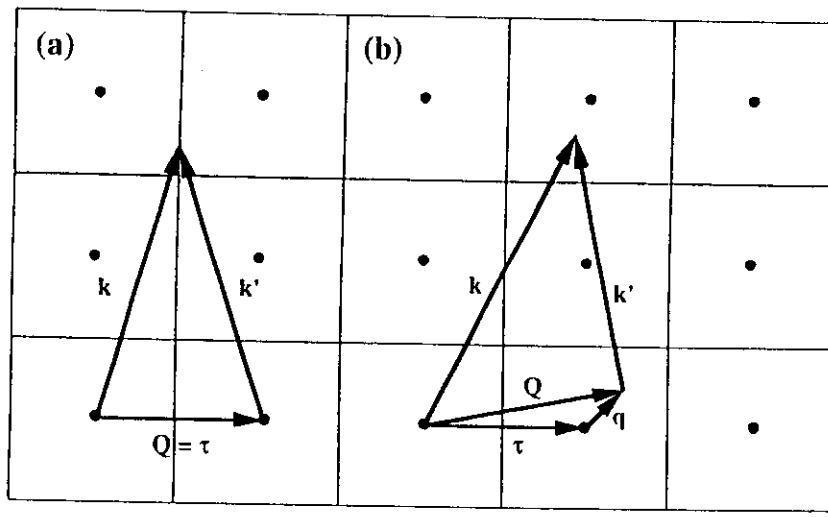

Fig. 3.1: Visualization of eq. (3.1) in reciprocal space for elastic (a) and inelastic (b) neutron scattering. The lines indicate the boundaries of the Brillouin zone, and the full circles denote the zone centers.

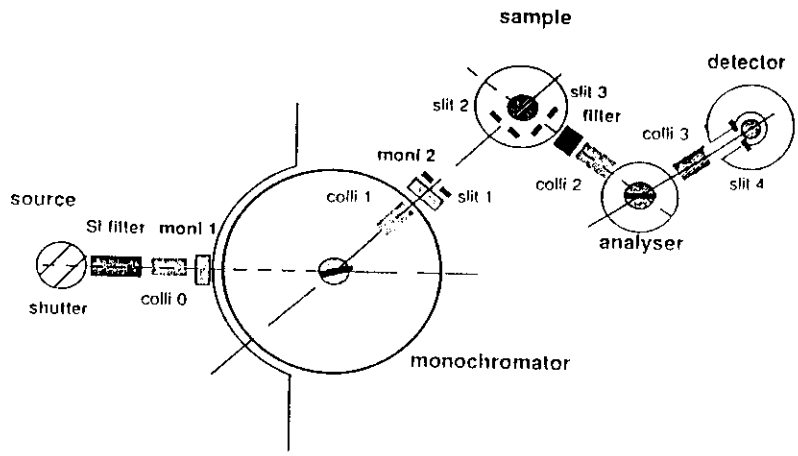

Fig. 3.2: Basic layout of a triple-axis spectrometer. The three axes around which the respective rest of the spectrometer is rotated are: the monochromator axis (variation of **k**), the sample axis (variation of the scattering angle), and the analyzer axis (variation of **k'**).

The determination of $\hbar\omega(\mathbf{q})$ by neutron scattering techniques requires a controlled access to the variables **Q** and ω. This can be done in various ways, but by far the most effective experimental method is the triple-axis crystal spectrometry developed by Brockhouse [2] who received the 1994 physics Nobel prize for this achievement. The principle of this method is sketched in Fig. 3.2. An incident beam of neutrons with a well defined wave vector **k** is selected from the white spectrum of the neutron source by the monochromator crystal, and scattered from the sample. The intensity of the scattered beam is measured as a function of **k'** by the analyzer crystal and the neutron detector.

The outstanding advantage of the triple-axis spectrometer is that data can be taken at predetermined points in reciprocal space (which is known as the "constant-**Q**" or "constant-ω" method), so that single-crystal measurements of the dispersion relation $\hbar\omega(\mathbf{Q})$ can be performed in a controlled manner. Of course, general scans in **Q** and ω are also possible.

For structural studies there is usually no need to perform an energy analysis by the third spectrometer axis. Neutron diffractometers are therefore called two-axis instruments. Advanced instruments often take advantage of position-sensitive detectors that speed up the rate of data collection tremendously.

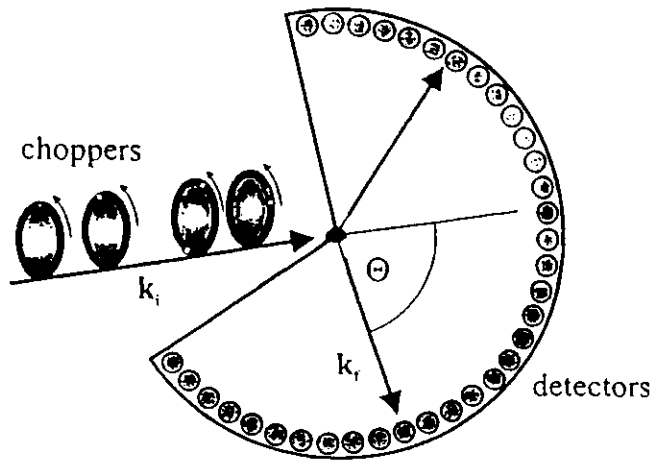

Fig. 3.3: Schematics of a direct time-of-flight spectrometer. The four choppers define the energy and the pulse width of the incident neutrons. In addition, they suppress higher-order neutrons and frame overlap.

For neutron scattering experiments on polycrystalline, liquid and amorphous materials various types of time-of-flight spectrometers are usually more appropriate. In the time-of-flight method the neutron beam is monochromated by a series of choppers

that produce pulses of neutrons with the desired wavelength and that eliminate higher-order neutrons and frame overlap of pulses from different repetition periods as well (see Fig. 3.3). The monochromatic neutron pulses are then scattered from the sample and are detected by arrays of neutron counters covering a large solid angle. The energy transfer $\hbar\omega$ and the modulus of the scattering vector **Q** are then determined by the flight time of the neutrons from the sample to the detector and the scattering angle at which the detector is positioned, respectively.

In the inverted time-of-flight method the white neutron beam is pulsed, for example by a spallation source itself, and the energy of the scattered neutrons is analysed by means of banks of analyser crystals or choppers. Recently, the time-of-flight method has also been successfully used for the measurement of excitations in single crystals (see ISIS 99 Progress Report, RAL, Didcot, UK).

4. Magnetic Neutron Cross-Section

The neutron scattering cross-section corresponds to the number of neutrons scattered per second into a (small) solid angle $d\Omega$ with energy transfers between $\hbar\omega$ and $\hbar(\omega+d\omega)$, divided by the flux of the incident neutrons. Theoretical expressions for the cross section usually start from Fermi's "golden rule"

$$\frac{d^2\sigma}{d\Omega d\omega} = \left(\frac{m}{2\pi\hbar^2}\right)^2 \frac{k'}{k} \sum_{\lambda} p_\lambda \sum_{\lambda'} |<\mathbf{k}',\lambda'|\hat{U}|\mathbf{k},\lambda>|^2 \delta(\hbar\omega + E_\lambda - E_{\lambda'}) \,. \qquad (4.1)$$

Here, $|\lambda>$ denotes the initial state of the scatterer, with energy E_λ and thermal population factor p_λ, and its final state is $|\lambda'>$. $\hat{U}$ is the interaction operator of the neutron with the sample which depends on the specific scattering process. E.g., neutron scattering from nuclei at fixed positions $\mathbf{R}_i$ is well approximated by the Fermi pseudopotential:

$$U(\mathbf{r}) = \frac{2\pi\hbar^2}{m} \sum_i b_i \delta(\mathbf{r} - \mathbf{R}_i) \,, \qquad (4.2)$$

where b_i is the scattering length. The magnitude of b_i is of the order 10^{-12} cm, i.e., for nuclear scattering the cross section (4.1) amounts to about 10^{-24} cm^2 (=1 barn).

For magnetic scattering the interaction operator $\hat{U}_m$ of the neutron with the sample may be described by the interaction of a neutron with a magnetic field **H**:

$$\hat{U}_m = \hat{\mu} \cdot \mathbf{H} = -\gamma \mu_N \hat{\sigma} \cdot \mathbf{H}, \tag{4.3}$$

where $\hat{\mu}$ is the magnetic moment operator of the neutron, γ=-1.91 the gyromagnetic ratio, μ_N=0.505·10^{-19} erg·T^{-1} the nuclear magneton, and $\hat{\sigma}$ a Pauli spin operator. For a large class of magnetic compounds the magnetic field **H** used in eq. (4.3) is generated by unpaired electrons. The magnetic field due to a single electron moving with velocity $\mathbf{v}_e$ is given by

$$\mathbf{H} = \mathrm{curl}\left\{\frac{\mu_e \times \mathbf{R}}{|\mathbf{R}|^3}\right\} - \frac{e}{c}\frac{\mathbf{v}_e \times \mathbf{R}}{|\mathbf{R}|^3}, \tag{4.4}$$

where **R** is the distance from the electron to the point at which the field is measured, e=1.602·10^{-19} C the elementary charge, and c=3·10^{10} cm·s^{-1} the velocity of light. The magnetic moment operator of an electron is

$$\hat{\mu}_e = -2\mu_B \hat{\mathbf{s}}, \tag{4.5}$$

where μ_B=0.927·10^{-16} erg·T^{-1} is the Bohr magneton and $\hat{\mathbf{s}}$ the spin operator of the electron. The first term of eq. (4.4) arises from the spin of the electron, and the second from its orbital motion.

The major task in the evaluation of the magnetic neutron cross-section is the calculation of the transition matrix element in eq. (4.1). This was first done by Halpern and Johnson [3], and more recently in many excellent text books on neutron scattering [4,5]. For unpolarized neutrons, identical magnetic ions with localized electrons, and spin-only scattering the following "**master formula**" is obtained:

$$\frac{d^2\sigma}{d\Omega d\omega} = (\gamma r_o)^2 \frac{k'}{k} F^2(\mathbf{Q}) \exp\{-2W(\mathbf{Q})\} \sum_{\alpha,\beta} \left(\delta_{\alpha\beta} - \frac{Q_\alpha Q_\beta}{Q^2} \right) S^{\alpha\beta}(\mathbf{Q},\omega) \ , \qquad (4.6a)$$

where $S^{\alpha\beta}(\mathbf{Q},\omega)$ is the magnetic scattering function:

$$S^{\alpha\beta}(\mathbf{Q},\omega) = \sum_{i,j} \exp\left\{ i\mathbf{Q} \cdot (\mathbf{R}_i - \mathbf{R}_j) \right\} \sum_{\lambda,\lambda'} p_\lambda < \lambda | \hat{S}_i^\alpha | \lambda' > < \lambda' | \hat{S}_j^\beta | \lambda > \delta(\hbar\omega + E_\lambda - E_{\lambda'}) \ . \qquad (4.6b)$$

r_o=0.282·10^{-12} cm is the classical electron radius, $F(\mathbf{Q})$ the dimensionless magnetic form factor defined as the Fourier transform of the normalized spin density associated with the magnetic ions, $\exp\{-2W(\mathbf{Q})\}$ the Debye-Waller factor, and $\hat{S}_i^\alpha$ (α=x,y,z) the spin operator of the *i*th ion at site $\mathbf{R}_i$. From the magnitude of r_o we expect the magnetic neutron cross section to be of the order 10^{-24} cm^{-2}, i.e., similar to the size of the nuclear cross section.

The essential factor in eq. (4.6) is the magnetic scattering function $S^{\alpha\beta}(\mathbf{Q},\omega)$ which will be discussed in more detail below. There are two further factors which govern the cross section for magnetic neutron scattering in a characteristic way: Firstly, the magnetic form factor $F(\mathbf{Q})$ which usually falls off with increasing modulus of the scattering vector $\mathbf{Q}$. Secondly, the polarization factor ($\delta_{\alpha\beta}$-$Q_\alpha Q_\beta/Q^2$) tells us that neutrons can only couple to magnetic moments or spin fluctuations perpendicular to $\mathbf{Q}$ which unambiguously allows to determine moment directions or to distinguish between different polarizations of spin fluctuations.

Eq. (4.6) strictly applies to cases where the orbital angular momentum of the magnetic ions is either zero or quenched by the crystal field. A theoretical treatment of the scattering by ions with unquenched orbital moment has been given by Johnston [6], however, the calculation is complicated, and we simply quote the result for $Q \rightarrow 0$. In this case the cross section measures the magnetisation, $\mu = -\mu_B(\mathbf{L}+2\mathbf{S})$, i.e., a combination of spin and orbital moments that does not allow their separation. This

clearly contrasts to magnetic scattering by X-rays. For magnetic neutron scattering an approximate result can be obtained for modest values of Q. We replace the spin operator $\hat{S}_i^\alpha$ in eq. (4.6) by

$$\hat{S}_i^\alpha = \tfrac{1}{2} g \hat{J}_i^\alpha \ , \tag{4.7}$$

where

$$g = 1 + \frac{J(J+1) - L(L+1) + S(S+1)}{2J(J+1)} \tag{4.8}$$

is the Landé splitting factor and $\hat{J}_i^\alpha$ is an effective angular momentum operator (e.g., for rare-earth ions J is the total angular momentum quantum number resulting from the spin-orbit coupling which combines the spin and orbital angular momentum L and S, respectively).

If ω is a positive quantity in the scattering function $S^{\alpha\beta}(\mathbf{Q},\omega)$ of eq. (4.6), the neutron loses energy in the scattering process and the system is excited from the initial state λ which has energy $\hbar\omega$ less than the final state λ'. Consider now the function $S^{\alpha\beta}(\mathbf{Q},-\omega)$ where ω is the same positive quantity. This represents a process in which the neutron gains energy. The transitions of the system are between the same states as for the previous process, but now λ' is the initial state and λ is the final state. The probability of the system being initially in the higher state is lower by the factor $\exp\{-\hbar\omega / k_B T\}$ than its probability of being in the lower energy state, hence

$$S^{\alpha\beta}(\mathbf{Q},-\omega) = \exp\left\{-\frac{\hbar\omega}{k_B T}\right\} S^{\alpha\beta}(\mathbf{Q},\omega) \ , \tag{4.9}$$

which is known as the **principle of detailed balance**. Eq. (4.9) has to be applied in the analysis of experimental data taken in both energy-gain and energy-loss configurations which correspond to the so-called Stokes and anti-Stokes processes, respectively.

Using the integral representation of the δ-function,

$$\delta(\hbar\omega + E_\lambda - E_{\lambda'}) = \frac{1}{2\pi\hbar}\int_{-\infty}^{+\infty} \exp\left\{i\frac{(E_{\lambda'} - E_\lambda)t}{\hbar}\right\}\exp\{-i\omega t\}dt \ , \qquad (4.10)$$

the scattering function $S^{\alpha\beta}(\mathbf{Q},\omega)$ (eq. 4.6) transforms into a physically transparent form:

$$S^{\alpha\beta}(\mathbf{Q},\omega) = \frac{1}{2\pi\hbar}\sum_{i,j}\int_{-\infty}^{+\infty}\exp\left\{i\mathbf{Q}\cdot(\mathbf{R}_i - \mathbf{R}_j)\right\} < \hat{S}_i^\alpha(0)\hat{S}_j^\beta(t) > \exp\{-i\omega t\}dt \ . \qquad (4.11)$$

$< \hat{S}_i^\alpha(0)\hat{S}_j^\beta(t) >$ is the thermal average of the time-dependent spin operators. It corresponds to the van Hove pair correlation function [7] and gives essentially the probability that, if the magnetic moment of the *ith* ion at site $\mathbf{R}_i$ has some specified (vector) value at time zero, then the moment of the *jth* ion at site $\mathbf{R}_j$ has some other specified value at time t. A neutron scattering experiment measures the Fourier transform of the pair correlation function in space and time, which is clearly just what is needed to describe a magnetic system on an atomic scale.

The van Hove representation of the cross section in terms of pair correlation functions is related to the fluctuation-dissipation theorem [4,5,8]:

$$S^{\alpha\beta}(\mathbf{Q},\omega) = \frac{N\hbar}{\pi}\left(1 - \exp\left\{-\frac{\hbar\omega}{k_B T}\right\}\right)^{-1} \mathrm{Im}\,\chi^{\alpha\beta}(\mathbf{Q},\omega) \ , \qquad (4.12)$$

where N is the total number of magnetic ions. Physically speaking, the neutron may be considered as a magnetic probe which effectively establishes a frequency- and wave vector-dependent magnetic field, $H^\beta(\mathbf{Q},\omega)$, in the scattering sample, and detects its response, $M^\alpha(\mathbf{Q},\omega)$, to this field by

$$M^\alpha(\mathbf{Q},\omega) = \chi^{\alpha\beta}(\mathbf{Q},\omega)H^\beta(\mathbf{Q},\omega) \ , \qquad (4.13)$$

where $\chi^{\alpha\beta}(\mathbf{Q},\omega)$ is the generalized magnetic susceptibility tensor. This is really the outstanding property of the neutron in a magnetic scattering measurement, and no other experimental technique is able to provide such detailed microscopic information about magnetic compounds.

5. Elastic Magnetic Neutron Scattering

5.1. Magnetic Structure Determination

We start from the master formula (4.6). For elastic scattering we have $|\lambda\rangle=|\lambda'\rangle$, so that the matrix elements in eq. (4.6b) can be replaced by their expectation values. With $\vec{\ell} = \vec{R}_j - \vec{R}_j$ and by integration with respect to ω we obtain

$$\frac{d\sigma}{d\Omega} = (\gamma r_o)^2 e^{-2W} \sum_{\alpha,\beta}\left(\delta_{\alpha\beta} - \frac{Q_\alpha Q_\beta}{Q^2}\right) F^2(\vec{Q}) \sum_{\vec{\ell}} e^{i\vec{Q}\cdot\vec{\ell}} \left\langle \hat{S}_o^\alpha \right\rangle \left\langle \hat{S}_{\vec{\ell}}^\beta \right\rangle \quad . \tag{5.1}$$

5.1.1. Paramagnets

For paramagnetic systems there is no correlation between the spins at sites 0 and $\vec{\ell}$, thus we have for $\ell \neq 0$

$$\left\langle \hat{S}_o^\alpha \right\rangle \left\langle \hat{S}_{\vec{\ell}}^\beta \right\rangle = 0 \quad . \tag{5.2}$$

Therefore we have to consider only the case $\ell = 0$. We find

$$< \hat{S}_o^\alpha >< \hat{S}_o^\beta >= \delta_{\alpha\beta} < \hat{S}_o^\alpha >< \hat{S}_o^\beta >= \delta_{\alpha\beta} < (\hat{S}_o^\alpha)^2 >= \tfrac{1}{3}\delta_{\alpha\beta} < \hat{\vec{S}} >^2 = \tfrac{1}{3}\delta_{\alpha\beta} S(S+1)$$

and (5.3)

$$\sum_{\alpha,\beta}\left(\delta_{\alpha\beta}-\frac{Q_\alpha Q_\beta}{Q^2}\right)=\sum_{\alpha}\left(1-\left(\frac{Q_\alpha}{Q}\right)^2\right)=2\ ,$$

thus the final cross section reads

$$\frac{d\sigma}{d\Omega}=\frac{2}{3}N(\gamma r_o)^2 e^{-2W}F^2(\vec{Q})S(S+1)\ . \tag{5.4}$$

5.1.2. Ferromagnets

A ferromagnet consists of domains with uniformly arranged spins, but the spin directions in each domain are different. Let us consider a single domain in which the spins are oriented along the z axis. Then

$$\langle\hat{S}_\ell^x\rangle=\langle\hat{S}_\ell^y\rangle=0\ ;\ \langle\hat{S}_\ell^z\rangle\neq 0\ . \tag{5.5}$$

For a Bravais ferromagnet we can skip the index ℓ and find from eqs. (5.1) and (5.5)

$$\frac{d\sigma}{d\Omega}=(\gamma r_o)^2 e^{-2W}F^2(\vec{Q})\left(1-\left(\frac{Q_z}{Q}\right)^2\right)\langle\hat{S}^z\rangle^2\sum_{\ell}e^{i\vec{Q}\cdot\vec{\ell}}\ . \tag{5.6}$$

Herein the lattice sum can be expressed as

$$\sum_{\ell}e^{i\vec{Q}\cdot\vec{\ell}}\ =\ \frac{(2\pi)^3}{v_o}\sum_{\tau}\delta(\vec{Q}-\vec{\tau})\ , \tag{5.7}$$

where v_o is the volume of the unit cell and $\vec{\tau}$ a reciprocal lattice vector. By defining $\vec{e}$ as the unit vector along the magnetisation direction z we can modify eq. (5.6) by

$$\frac{Q_z}{Q} = \frac{\vec{Q}\cdot\vec{e}}{Q} = \frac{\vec{\tau}\cdot\vec{e}}{\tau} \tag{5.8}$$

and arrive at the final formula for the cross section:

$$\frac{d\sigma}{d\Omega} = N\frac{(2\pi)^3}{v_o}(\gamma r_o)^2 e^{-2W} F^2(\vec{Q})\langle\hat{S}^z\rangle^2 \sum_{\vec{\tau}}\left\langle 1-\left(\frac{\vec{\tau}\cdot\vec{e}}{\tau}\right)^2\right\rangle \delta(\vec{Q}-\vec{\tau}) \,. \tag{5.9}$$

The $\langle\ \rangle$ brackets denote the average over all the domain orientations which for an arbitrary distribution of domain orientations reduces to

$$\left\langle 1-\left(\tfrac{\vec{\tau}\cdot\vec{e}}{\tau}\right)^2\right\rangle = \tfrac{2}{3} \,. \tag{5.10}$$

Equation (5.10) also holds if for symmetry reasons only a few domain orientations are possible, e.g., (100), (010), and (001) in systems of cubic symmetry.

Eq. (5.9) shows that ferromagnetic Bragg scattering occurs at all the reciprocal lattice vectors, thus it is often difficult to separate the ferromagnetic from the nuclear Bragg scattering. A discrimination between the two scattering contributions can be achieved by considering the essential factors in eq. (5.9):

- The magnetic Bragg scattering is proportional to the square of the zero-field magnetisation, $<\hat{S}^z>^2$, which exhibits a strong temperature dependence, particularly when approaching the Curie temperature.
- The $\vec{Q}$-dependence of the magnetic scattering follows the square of the magnetic form factor, $F^2(\vec{Q})$, which decreases rapidly with increasing modulus of $\vec{Q}$.
- The magnetic scattering depends on the orientation of $<\vec{S}^z>$ relative to the reciprocal lattice vector $\vec{\tau}$.

Furthermore, by applying an external magnetic field along $\vec{Q}$ the spins will align along that direction (for sufficiently large fields), so that $\frac{\vec{\tau}\cdot\vec{e}}{\tau} = 1$, thus the magnetic scattering vanishes. The difference of two measurements (with and without external field) yields therefore directly the magnetic scattering contributions. The most elegant method for

discrimination, however, involves the use of polarised neutrons, see lecture by F. Tasset.

5.1.3. Antiferromagnets

In antiferromagnets the domains consist of two sublattices A und B with antiparallel spin alignment, thus $< \hat{S}^z >= 0$ in each domain. One therefore defines $< \hat{S}^z >$ as the so-called staggered spin, i.e., the zero-field magnetisation in each of the two sublattices A and B. For the calculation of the cross section we start from eq. (5.6) by defining a new magnetic unit cell (with volume v_{om}) which is the unit cell of the sublattice A (including the spin of the sublattice B at site $\vec{d}$):

$$\frac{d\sigma}{d\Omega} = (\gamma r_o)^2 e^{-2W} F^2(\vec{Q}) \left(1 - \left(\frac{Q_z}{Q}\right)^2\right) \left\langle \hat{S}^z \right\rangle^2 \sum_A e^{i\vec{Q}\cdot\vec{l}} \sum_d \sigma_d e^{i\vec{Q}\cdot\vec{d}} \quad . \tag{5.11}$$

$\sigma_d = +1$ for an ion in sublattice A and $\sigma_d = -1$ for an ion in sublattice B. By using eq. (5.7) we find the final cross-section formula:

$$\frac{d\sigma}{d\Omega} = N_m \frac{(2\pi)^3}{v_{om}} (\gamma r_o)^2 e^{-2W} \sum_{\vec{\tau}_m} \left|F_m(\vec{\tau}_m)\right|^2 \left\langle 1 - (\vec{\tau}_m \cdot \vec{e})^2 \right\rangle \delta(\vec{Q} - \vec{\tau}_m) \tag{5.12a}$$

with the magnetic structure factor

$$F_m(\vec{\tau}_m) = \left\langle \hat{S}^z \right\rangle F(\vec{\tau}_m) \sum_d \sigma_d e^{i\vec{\tau}_m \cdot \vec{d}} \quad . \tag{5.12b}$$

$\vec{\tau}_m$ denotes a magnetic reciprocal lattice vector.

Let us consider as an example the antiferromagnet $KMnF_3$ (T_N=83K). The chemical lattice has simple cubic symmetry (see Fig 5.1), thus the reciprocal lattice has also simple cubic symmetry, and the reciprocal lattice vectors are defined by $\vec{\tau} = \frac{2\pi}{a}(t_1, t_2, t_3)$, with integer numbers t_i. The magnetic lattice, however, is face-centered cubic, thus the magnetic reciprocal lattice has body-centered cubic symmetry. According to Fig. 5.1 the magnetic reciprocal lattice vectors are defined by $\vec{\tau}_m = \frac{2\pi}{a}(t_1, t_2, t_3)$ or $\vec{\tau}_m = \frac{2\pi}{a}(t_1 + \frac{1}{2},\ t_2 + \frac{1}{2},\ t_3 + \frac{1}{2})$. From eq. (5.12) we find:

$$\sum_d \sigma_d e^{i\vec{\tau}_m \cdot \vec{d}} = 0 \text{ for } \vec{\tau}_m = \frac{2\pi}{a}(t_1, t_2, t_3) \ ,$$

$$= 2 \text{ for } \vec{\tau}_m = \frac{2\pi}{a}\left(t_1 + \tfrac{1}{2}, t_2 + \tfrac{1}{2}, t_3 + \tfrac{1}{2}\right) \ .$$

We arrive at the important result that nuclear and magnetic Bragg scattering occurs at different points in the reciprocal lattice. This is visualised in Fig. 5.2 for the neutron diffraction pattern taken for $KMnF_3$ at T= 4.2 K.

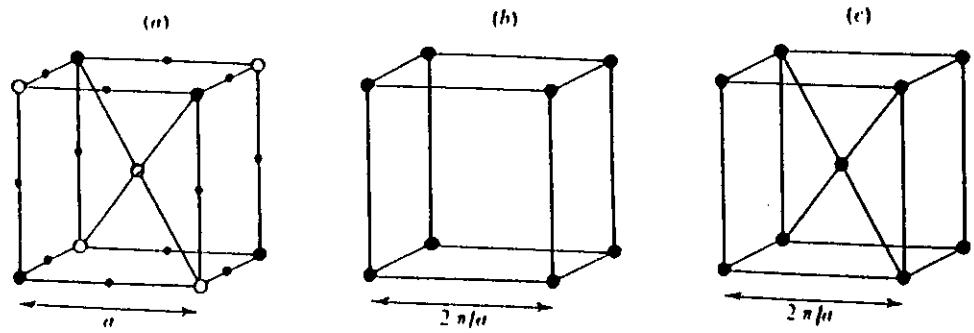

Fig. 5.1 (a) Structure of $KMnF_3$. (b) Chemical reciprocal lattice (all Mn ions are identical). (c) Magnetic reciprocal lattice.

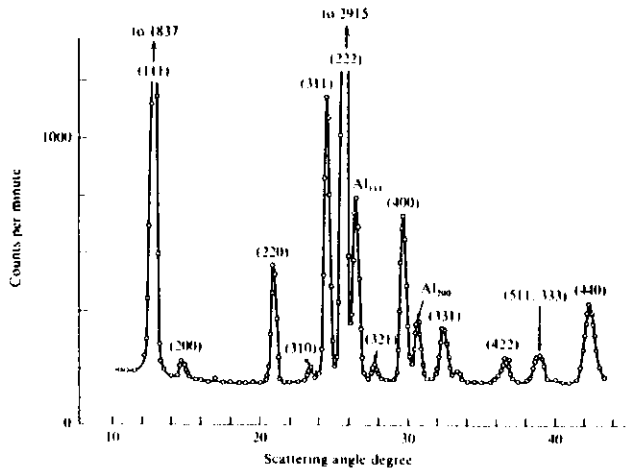

Fig. 5.2: Neutron diffraction pattern of $KMnF_3$ at 4.2 K [V. Scatturin et al., Acta Cryst. **14**, 19 (1961)]. The numbers by the peaks are the coordinates in reciprocal space multiplied by 2. A trio of odd numbers represents a magnetic peak, a trio of even numbers a nuclear peak.

5.1.4. Helical Spin Structures (Magnetic Spiral Structures)

Let us consider the magnetic spiral structure of Au_2Mn (magnetic ordering temperature = 363 K) as shown in Fig. 5.3. The Mn ions form a body-centered tetragonal lattice.

Within a plane perpendicular to the z axis all the moments are ferromagnetically aligned, but the moment direction turns by an angle ϕ between adjacent planes. We define a spiral vector $\vec{P}$ as follows: $\vec{P}$ is a vector along the z axis; its length equals $\frac{2\pi}{\Phi}$-times the distance d between adjacent planes. The expectation values of the spin operators are then given by

$$\begin{aligned} &<\hat{S}_\ell^x> = <\hat{\vec{S}}> \cos(\vec{P}^* \cdot \vec{\ell}), \\ &<\hat{S}_\ell^y> = <\hat{\vec{S}}> \sin(\vec{P}^* \cdot \vec{\ell}), \\ &<\hat{S}_\ell^z> = 0, \end{aligned} \tag{5.13}$$

with $P^* = \frac{2\pi}{P}$. Inserting in eq. (5.1) yields

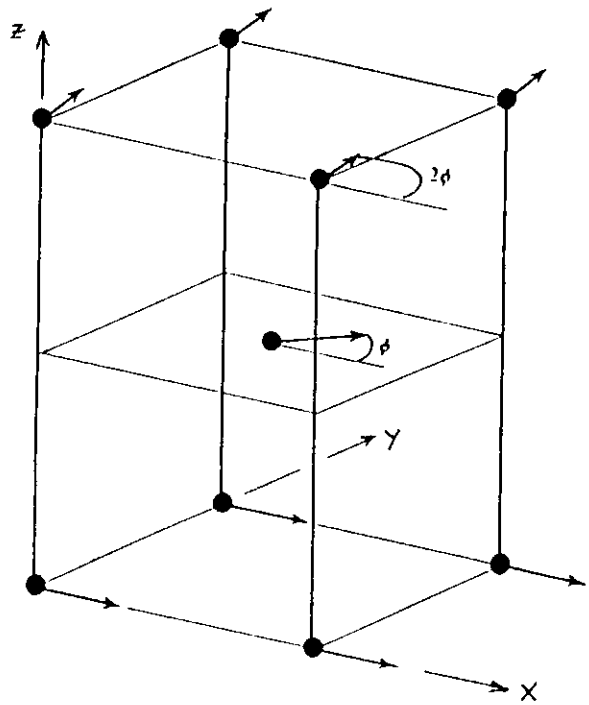

Fig. 5.3: Structure of Au_2Mn (only the Mn ions are shown).

$$\frac{d\sigma}{d\Omega} = (\gamma r_o)^2 e^{-2W} F^2(\vec{Q}) \sum_{\vec{\ell}} e^{i\vec{Q}\cdot\vec{\ell}} \left\langle \hat{\vec{S}} \right\rangle^2 \left\{ \left(1 - \left(\frac{Q_x}{Q}\right)^2\right) \cos\left(\vec{P}^* \cdot \vec{\ell}\right) - \frac{Q_x Q_y}{Q^2} \sin\left(\vec{P}^* \cdot \vec{\ell}\right) \right\} . \tag{5.14}$$

Since $\vec{P}^*$ is not a reciprocal lattice vector, the summation over $\sin(\vec{P}^* \cdot \vec{\ell})$ vanishes. We express $\cos(\vec{P}^* \cdot \vec{\ell})$ by an exponential:

$$\frac{d\sigma}{d\Omega} = (\gamma r_o)^2 e^{-2W} F^2(\vec{Q}) \left\langle \hat{\vec{S}} \right\rangle^2 \left(1 - \left(\frac{Q_x}{Q}\right)^2\right) \frac{1}{2} \sum_{\vec{\ell}} \left(e^{i(\vec{Q}+\vec{P}^*)\cdot\vec{\ell}} + e^{i(\vec{Q}-\vec{P}^*)\cdot\vec{\ell}} \right) . \qquad (5.15)$$

Application of eq. (5.7) yields

$$\frac{d\sigma}{d\Omega} = \frac{N}{2} \frac{(2\pi)^3}{v_o} (\gamma r_o)^2 e^{-2W} F^2(\vec{Q}) \left\langle \hat{\vec{S}} \right\rangle^2 \left(1 - \left(\frac{Q_x}{Q}\right)^2\right) \sum_{\vec{\tau}} \left\{ \delta(\vec{Q} + \vec{P}^* - \vec{\tau}) + \delta(\vec{Q} - \vec{P}^* - \vec{\tau}) \right\} . \qquad (5.16)$$

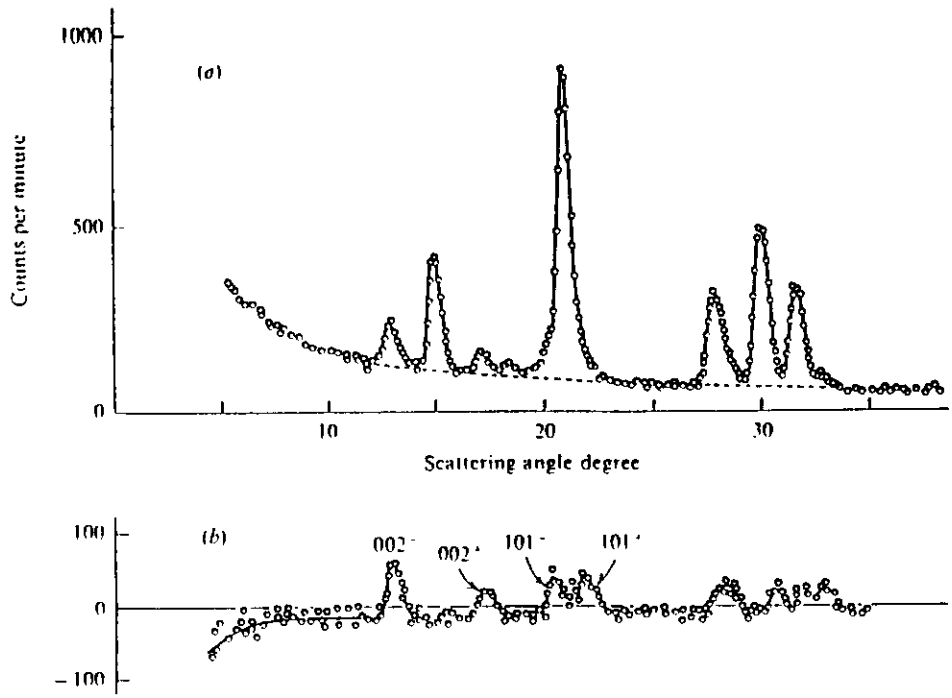

Fig. 5.4: Neutron diffraction pattern taken for Au_2Mn [A. Herpin et al., Comptes Rendus **249**, 1334 (1959)]. (a) T=293 K. (b) Difference of spectra taken at 293 K and 423 K.

The assumptions of eq. (5.13) were somehow special in the sense that we confined the moment direction to the x axis in the basal plane. We could as well start with the

moment direction along the y axis, which would change the polarisation factor in eq. (5.16) from $\left[1-\left(\frac{Q_x}{Q}\right)^2\right]$ to $\left[1-\left(\frac{Q_y}{Q}\right)^2\right]$. Taking the average yields the final cross section

$$\frac{d\sigma}{d\Omega}=\frac{N}{4}\frac{(2\pi)^3}{v_o}(\gamma r_o)^2 e^{-2W}F^2(\vec{Q})\left\langle\hat{\vec{S}}\right\rangle^2\left(1+\left(\frac{Q_z}{Q}\right)^2\right)\sum_{\vec{\tau}}\left\{\delta(\vec{Q}+\vec{P}^*-\vec{\tau})+\delta(\vec{Q}-\vec{P}^*-\vec{\tau})\right\}. \quad (5.17)$$

We realise that magnetic Bragg scattering occurs for $\vec{Q}=\vec{\tau}\pm\vec{P}^*$, i.e., each nuclear Bragg reflection is flanked by a pair of magnetic satellites. This is visualised in Fig. 5.4 for Au_2Mn.

5.1.5. The Magnetic Ordering Wavevector

Besides the examples treated above there is a myriad of other magnetic structure types. It is convenient to characterise them by the magnetic ordering wave-vector $\vec{q}_o$ which is defined by the relation

$$\vec{\mu}_i=\vec{\mu}_o\cos(\vec{q}_o\cdot\vec{R}_i)\,, \quad (5.18)$$

i.e., $\vec{q}_o$ describes properly the mutual orientation of the magnetic moments at sites 0 und $\vec{R}_i$. For instance, for the antiferromagnet $KMnF_3$ described in Chapter 5.1.3 we have $\vec{q}_o=\frac{2\pi}{a}(\frac{1}{2},\frac{1}{2},\frac{1}{2})$.

5.1.6. Zero-Field Magnetisation

An inherent factor in all the cross-section formulae derived above is the square of the expectation value of the spin operator $\hat{\vec{S}}$, see eq. (5.9) for the ferromagnet, eq. (5.12) for

the antiferromagnet, and eq. (5.17) for the spiral structure. The expectation value of the spin operator $\hat{\vec{S}}$ is directly related to the magnetic moment $\vec{\mu}$:

$$\vec{\mu} = g\mu_B < \hat{\vec{S}} > , \tag{5.19}$$

where g denotes the Landé-factor and μ_B the Bohr magneton. This means that the magnetic moment can be determined directly by neutron diffraction without the need to apply an external magnetic field (as in conventional magnetisation experiments). This property, namely the ability to measure the magnetisation without a disturbing magnetic field (therefore the term "zero-field magnetisation"), is unique for neutron scattering.

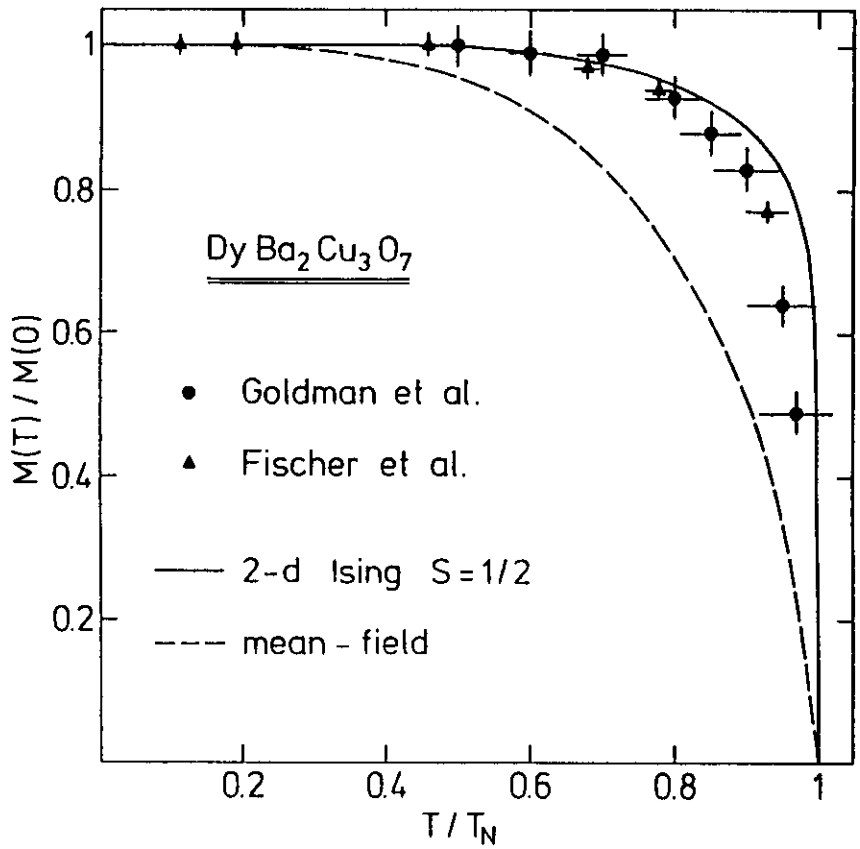

Fig. 5.5: Zero-field magnetisation of the Dy^{3+} ions in $DyBa_2Cu_3O_7$ [Allenspach et al., Phys. Rev. B **39**, 2226 (1989)].

5.2. Vortices in Type-II Superconductors

A flux-line lattice forms inside a type-II superconductor when the applied field H is sufficient to cause vortices to enter ($>H_{c1}$) but insufficient to destroy superconductivity altogether ($<H_{c2}$). According to Abrikosov [9] the flux lines are oriented parallel to the applied field and form a two-dimensional lattice. The Bragg d-spacing of a flux-line lattice is given by the condition that there is one flux quantum $\Phi_o=2.07\times10^{-15}$ Wb per unit cell, and hence

$$d = \sqrt{\Phi_o / B} \tag{5.20}$$

for a square lattice and

$$d = \sqrt{\sqrt{3}\Phi_o / 2B} \tag{5.21}$$

for a triangular lattice. For B=0.2 T this gives d≈1000 Å, and with an incident neutron wavelength λ=10 Å we have a Bragg angle 2Θ≈0.5°. This means that the small angle neutron scattering (SANS) technique has to be applied.

The diffraction of neutrons by flux lines occurs essentially by the same principles as discussed in Chapter 5.1. The neutron cross-section is proportional to the square of the form factor F_{hk} which is the Fourier transform of the flux-line distribution $h(\vec{r})$ in the sample:

$$F_{hk} = \frac{1}{\Phi_o}\int h(\vec{r})e^{i\vec{\tau}_{hk}\cdot\vec{r}}d\vec{r} \ . \tag{5.22}$$

For more detailed information on SANS experiments of flux-line lattices in type-II superconductors we refer to a recent review article by E.M. Forgan [10]. Figs (5.6) and (5.7) exemplify the procedure for the determination of the flux-line lattice in Nb.

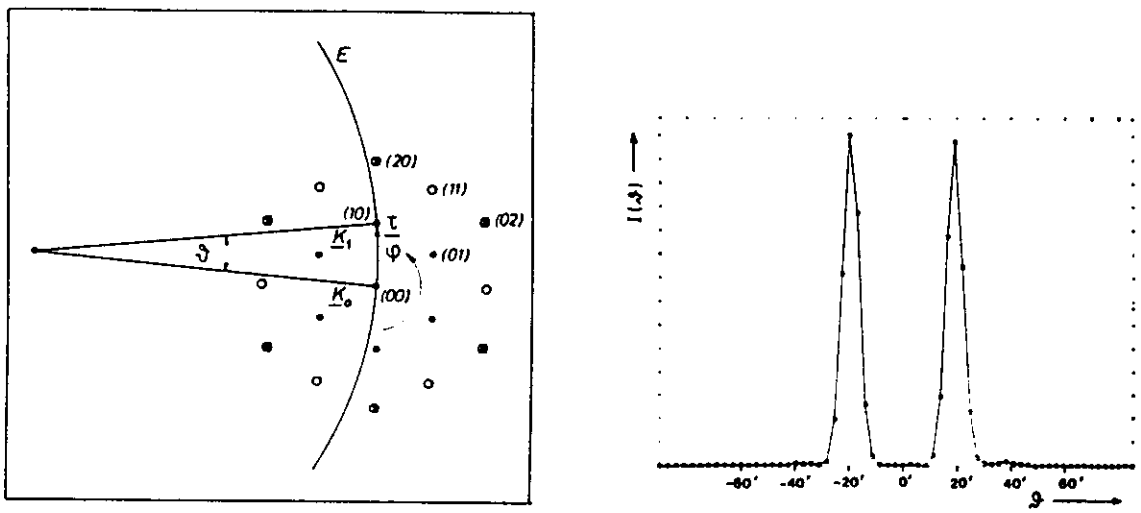

Fig. 5.6: Left hand side: Geometry of the scattering process for neutron diffraction from a triangular flux-line lattice. E denotes the Ewald sphere. Right hand side: Neutron diffraction pattern observed for the d_{10} reflections in Nb [Lippmann et al., J. Appl. Cryst. 7, 236 (1974)].

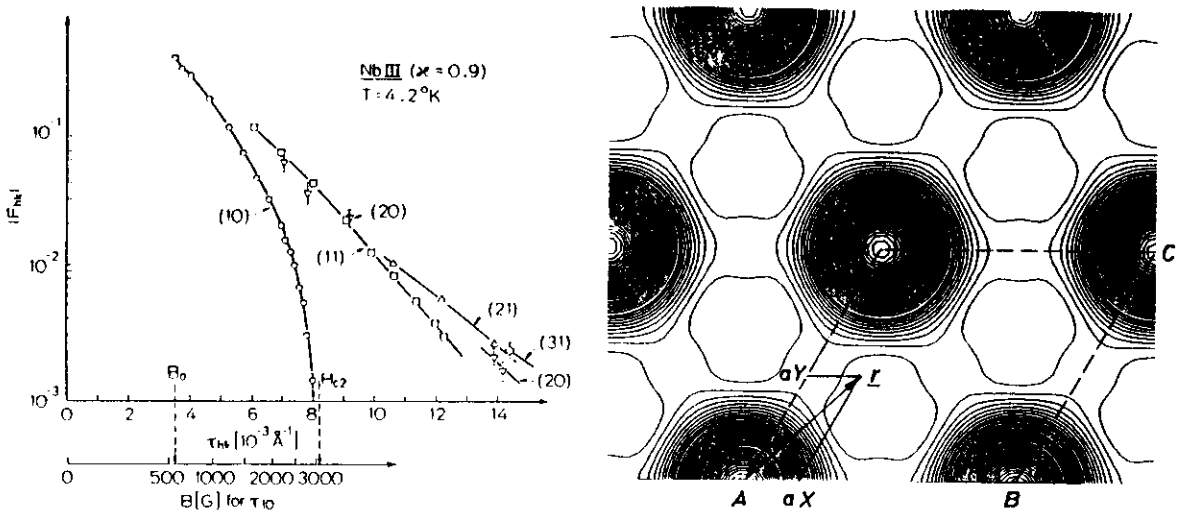

Fig. 5.7: Left hand side: Form factors observed for the flux-line lattice in Nb. Right hand side: Flux-line distribution $h(\vec{r})$ in Nb determined by a Fourier transformation of the measured form factors [Schelten et al., Z. Phys. **253**, 219 (1972)].

6. Inelastic Magnetic Neutron Scattering

6.1. Single-Ion Crystal-Field Excitations

If the coupling between the magnetic ions is weak, we are left with a single-ion problem, thus the excitation energies will be independent of the scattering vector **Q**. Typical examples are rare-earth compounds which exhibit very low magnetic ordering temperatures or do not order at all. In this case the dominant mechanism is the crystal-field interaction.

The effect of the crystal field on a rare-earth ion is to partially or totally remove the (2J+1)-fold degeneracy of the ground-state J-multiplet. This is exemplified at the top of Fig. 6.1 for Pr^{3+} ions in the hexagonal compound $PrBr_3$.[1] The crystal-field levels are denoted by the irreducible representations Γ_n, and the corresponding wave functions are

$$|\Gamma_n> \; = \; \sum_{M=-J}^{J} a_n(M) \; |M> \; . \tag{6.1}$$

From the sequence of the energy levels, properly identified by their irreducible representations Γ_n, the crystal-field potential can be unambiguously determined.

In evaluating the cross-section for the crystal-field transition $\Gamma_n \rightarrow \Gamma_m$ we start from the scattering law $S^{\alpha\beta}(\mathbf{Q},\omega)$ defined by eq. (4.6). Since we are dealing with single-ion excitations, we have i=j. For N identical magnetic ions we can even drop the index i. $S^{\alpha\beta}(\mathbf{Q},\omega)$ then reduces to

$$S^{\alpha\beta}(\omega) \; = \; N \; p_{\Gamma_n} <\Gamma_n \; |\hat{J}^{\alpha}|\Gamma_m><\Gamma_m \; |\hat{J}^{\beta}|\; \Gamma_n> \; \delta(\hbar\omega + E_{\Gamma_n} - E_{\Gamma_m}) \; , \tag{6.2}$$

where N is the total number of magnetic ions and p_{Γ_n} the Boltzmann population factor. From the symmetry relations associated with the matrix elements we find the cross section

$$\frac{d^2\sigma}{d\Omega d\omega} = N\left(\tfrac{1}{2}g\gamma r_o\right)^2 \frac{k'}{k} F^2(\mathbf{Q})\, \exp\{-2W(\mathbf{Q})\}\, p_{\Gamma_n} \sum_\alpha \left(1-\frac{Q_\alpha^2}{Q^2}\right) |<\Gamma_m|\hat{J}^\alpha|\Gamma_n>|^2\, \delta(\hbar\omega + E_{\Gamma_n} - E_{\Gamma_m}) \,. \tag{6.3}$$

The polarization factor permits discrimination between transverse (α=x,y) and longitudinal (α=z) crystal-field transitions by measuring at different **Q**. This is nicely demonstrated in Fig. 6.1. E.g., for **Q**||c only transverse transitions are observed, whereas for **Q**⊥c the transverse transitions lose half their intensities, and in addition longitudinal transitions appear. The lines in Fig. 6.1 were calculated without any disposable parameters, i.e., the intensities of the crystal-field transitions are excellently described by eq. (6.3).

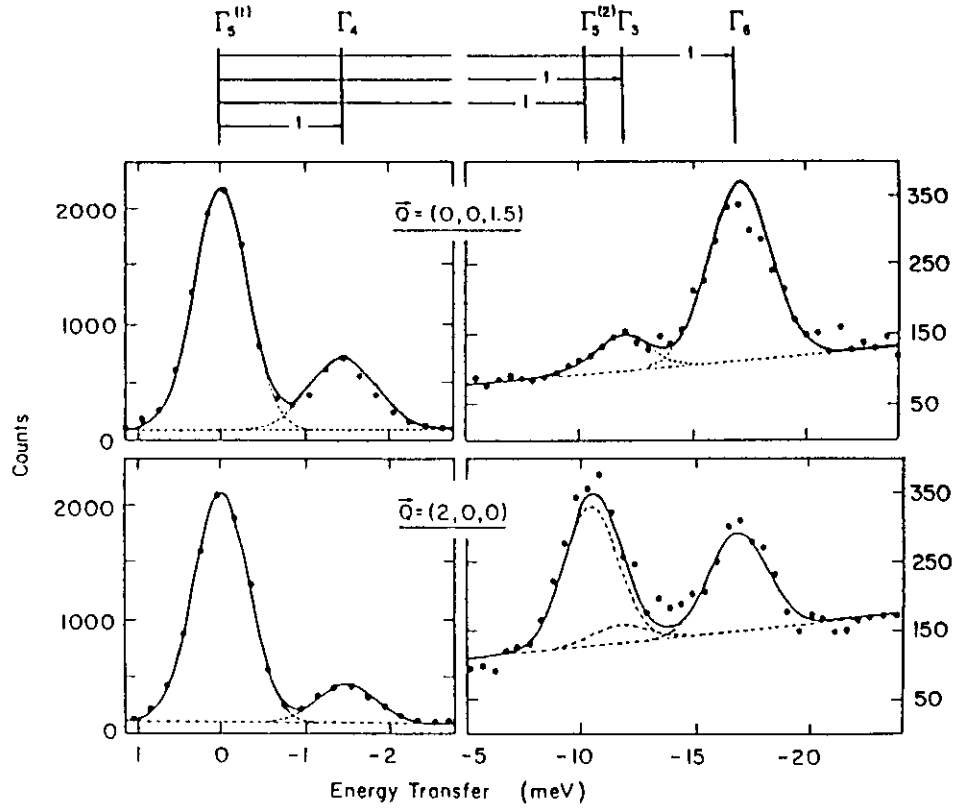

Fig. 6.1: Energy spectra of neutrons scattered from single-crystalline $PrBr_3$ at T=1.5 K for **Q** parallel and perpendicular to the c-axis [Schmid et al., J. Appl. Phys. **61**, 3426 (1987)]. The resulting crystal-field level scheme and the observed transverse (t) and longitudinal (l) ground-state transitions are indicated at the top.

For experiments on polycrystalline material eq. (6.3) has to be averaged in **Q** space:

$$\frac{d^2\omega}{d\Omega d\omega} = N\,(\tfrac{1}{2}g\gamma r_o)^2 \frac{k'}{k} F^2(Q)\, \exp\{-2W(Q)\}\; p_{\Gamma_n} |<\Gamma_m|\hat{\mathbf{J}}_\perp|\Gamma_n>|^2 \\ \delta(\hbar\omega + E_{\Gamma_n} - E_{\Gamma_m}) \;, \tag{6.4}$$

where $\mathbf{J}_\perp=\mathbf{J}-(\mathbf{J}\cdot\mathbf{Q})\,\mathbf{Q}/Q^2$ is the component of the total angular momentum perpendicular to the scattering vector **Q**, and

$$|<\Gamma_m|\hat{\mathbf{J}}_\perp|\Gamma_n>|^2 = \frac{2}{3}\sum_\alpha |<\Gamma_m|\hat{J}^\alpha|\Gamma_n>|^2 \;. \tag{6.5}$$

6.2. Magnetic Cluster Excitations

The simplest magnetic cluster system is the dimer (two coupled spins $\mathbf{S}_1$ and $\mathbf{S}_2$) for which the Heisenberg Hamiltonian is defined by

$$\hat{\mathcal{H}} = -2J\;\hat{\mathbf{S}}_1\cdot\hat{\mathbf{S}}_2 \;, \tag{6.6}$$

where J is the exchange integral. $\hat{\mathcal{H}}$ commutes with the total spin $\mathbf{S}=\mathbf{S}_1+\mathbf{S}_2$, thus S is a good quantum number. The wave functions of the dimer states are of the form |SM>. Assuming identical magnetic ions ($S_1=S_2$) the eigenvalues of eq. (6.6) are

$$E_S = -J\left[S(S+1)-2S_1(S_1+1)\right] \;,\; 0\le S\le 2S_1 \;. \tag{6.7}$$

The energy-level sequence of an antiferromagnetically coupled pair of ions with half-integer spin quantum number S_i is indicated at the right hand side of Fig. 6.2.

The calculation of the cross section for dimer excitations starts from eq. (4.6). For the evaluation of the matrix elements we replace the spin operators $\hat{S}_i^\alpha$ by irreducible tensor operators $\hat{T}_i^q$ of rank 1:

$$\hat{T}_i^o = \hat{S}_i^z \ , \quad \hat{T}_i^{\pm 1} = \mp \frac{1}{\sqrt{2}} \left(\hat{S}_i^x \pm i\hat{S}_i^y \right) . \tag{6.8}$$

The M dependence of the matrix elements is given by the Wigner-Eckart theorem:

$$\begin{aligned}
&< S'M' | \hat{T}_i^q | SM > = (-1)^{S'-M'} \begin{pmatrix} S' & 1 & S \\ -M' & q & M \end{pmatrix} < S' \| \hat{T}_i \| S > \ , \\
&< S' \| \hat{T}_1 \| S > = (-1)^{2S_1+S+1} \sqrt{(2S+1)(2S'+1)} \begin{Bmatrix} S' & S & 1 \\ S_1 & S_1 & S_1 \end{Bmatrix} < S_1 \| \| \hat{T}_1 \| \| S_1 >, \\
&< S' \| \hat{T}_2 \| S > = (-1)^{S-S'} < S' \| \hat{T}_1 \| S > \ , \\
&< S_1 \| \| \hat{T}_1 \| \| S_1 > = \sqrt{S_1(S_1+1)(2S_1+1)} \ .
\end{aligned} \tag{6.9}$$

From the symmetry properties of the 3j- and 6j-symbols in eq. (6.9) the selection rules

$$\Delta S = S - S' = 0, \pm 1 \ ; \quad \Delta M = M - M' = 0, \pm 1 \tag{6.10}$$

are derived. Thus inelastic transitions are only possible between adjacent energy levels (this follows immediately from eq. 6.7). Since each energy level is (2S+1)-fold degenerate, we can sum over the quantum numbers M and M':

$$\sum_{M,M'} < SM | \hat{T}_i^q | S'M' >< S'M' | \hat{T}_j^q | SM > = \frac{1}{3} < S \| \hat{T}_i \| S' >< S' \| \hat{T}_j \| S > \ . \tag{6.11}$$

Furthermore, we make use of the symmetry relations associated with the matrix elements defined by eq. (6.9). We then find the following cross section for the dimer transition $|S> \rightarrow |S'>$:

$$\frac{d^2\sigma}{d\Omega d\omega} = N\,(\gamma r_0)^2\,\frac{k'}{k}\,F^2(\mathbf{Q})\,\exp\{-2W(\mathbf{Q})\}\,p_s\sum_\alpha\left(1-\frac{Q_\alpha^{\,2}}{Q^2}\right) \frac{2}{3}\left[1+(-1)^{\Delta S}\cos(\mathbf{Q}\cdot\mathbf{R})\right]\,|<S'||\hat{T}_1||S>|^2\;\delta(\hbar\omega+E_s-E_{s'})\,, \tag{6.12}$$

where N is the total number of dimers, p_S the Boltzmann population factor, and **R** the intradimer separation. The structure factor $[1+(-1)^{\Delta S}\cos(\mathbf{Q}\cdot\mathbf{R})]$ is a powerful means to unambiguously identify dimer excitations from other scattering contributions due to its characteristic oscillating behaviour. This is nicely demonstrated in Fig. 6.2 by the **Q** dependence of the magnetic excitations of Mn^{2+} pairs (with **R**||c) introduced into a single crystal of $CsMgBr_3$. From the cross section (6.12) we calculate the intensity ratios of the transitions $0\rightarrow 1\,/\,1\rightarrow 2\,/\,2\rightarrow 3$ to be 1.0 / 0.9 / 0.3, in excellent agreement with the observations (see Fig. 6.2). The exchange coupling *J* between the Mn^{2+} ions (with S_i=5/2) is directly related to the energies of the observed dimer transitions, see eq. (6.7).

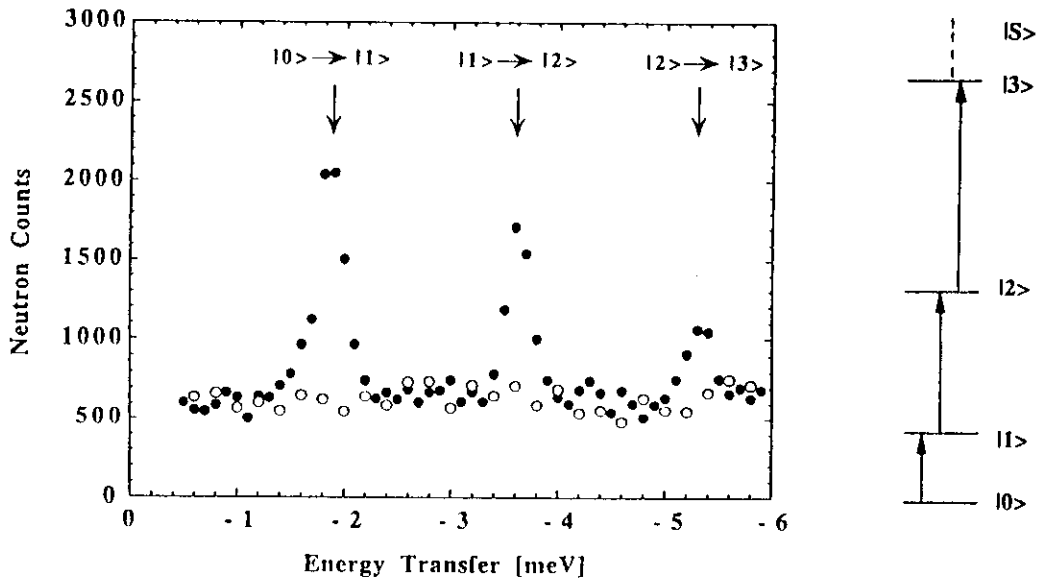

Fig. 6.2: Energy spectra of neutrons scattered from Mn^{2+} pairs in $CsMn_{0.28}Mg_{0.72}Br_3$ at T=30 K [Falk et al., Phys. Rev. Lett. **52**, 1336 (1984)]. Full circles: Q=(0,0,1); open circles: Q=(0,0,2).

For polycrystalline material eq. (6.12) has to be averaged in **Q** space:

$$\frac{d^2\sigma}{d\Omega d\omega} = N\,(\gamma r_o)^2\,\frac{k'}{k}\,F^2(Q)\,\exp\{-2W(Q)\}\;p_s \qquad \frac{4}{3}\left[1+(-1)^{\Delta s}\,\frac{\sin(QR)}{QR}\right]\,|<S'||\hat{T}_1||S>|^2\;\delta(\hbar\omega+E_s-E_{s'})\;. \tag{6.13}$$

6.3. Spin Waves

For an extended system the Heisenberg Hamiltonian (eq. 6.6) is written

$$\hat{\mathcal{H}} = -2\sum_{i>j} J_{ij}\;\hat{\mathbf{S}}_i\cdot\hat{\mathbf{S}}_j\;. \tag{6.14}$$

The exchange coupling J_{ij} forces the spins to be perfectly aligned (along the quantization axis z) at zero temperature. At finite temperatures spin deviations occur which propagate through the lattice giving rise to spin waves. The spin-wave dispersion is given by

$$\hbar\omega(\mathbf{q}) = 2S\;[\mathcal{J}(0)-\mathcal{J}(\mathbf{q})] \tag{6.15}$$

with the Fourier transformed exchange function

$$\mathcal{J}(\mathbf{q}) = \sum_{i,j} J_{ij}\;\exp\left\{i\mathbf{q}\cdot(\mathbf{R}_i-\mathbf{R}_j)\right\}\;. \tag{6.16}$$

The operators affecting the spin deviation of the *ith* atom (at site $\mathbf{R}_i$) are defined by

$$\begin{aligned}
\hat{S}_i^+(t) &= \sqrt{\frac{2S}{N}}\;\sum_{\mathbf{q}}\exp\left\{i\left[\mathbf{q}\cdot\mathbf{R}_i-\omega(\mathbf{q})t\right]\right\}\;\hat{a}_{\mathbf{q}}\;,\\
\hat{S}_i^-(t) &= \sqrt{\frac{2S}{N}}\;\sum_{\mathbf{q}}\exp\left\{-i\left[\mathbf{q}\cdot\mathbf{R}_i-\omega(\mathbf{q})t\right]\right\}\;\hat{a}_{\mathbf{q}}^+\;,\\
\hat{S}_i^z(t) &= S-\frac{1}{N}\;\sum_{\mathbf{q},\mathbf{q}'}\exp\left\{-\left[(\mathbf{q})-\mathbf{q}'\right)\cdot\mathbf{R}_i-(\omega(\mathbf{q})-(\omega(\mathbf{q}'))t\right]\right\}\;\hat{a}_{\mathbf{q}}^+\hat{a}_{\mathbf{q}}\;,
\end{aligned} \tag{6.17}$$

where

$$\hat{a}_q|n_q> = \sqrt{n_q}\,|n_q-1> \;;\; \hat{a}_q^+|n_q> = \sqrt{n_q+1}\,|n_q+1> \tag{6.18}$$

are annihilation and creation operators first introduced into spin-wave theory by Holstein and Primakoff [11]. With $<\hat{a}_q^+\hat{a}_q>=<n_q>$, $<\hat{a}_q\hat{a}_q^+>=<n_q+1>$ and the definitions

$$\hat{S}^x = \frac{1}{2}(\hat{S}^+ + \hat{S}^-) \;;\; S^y = -\frac{i}{2}(\hat{S}^+ - \hat{S}^-) \tag{6.19}$$

we calculate the spin correlation functions $<\hat{S}_i^\alpha(0)\hat{S}_j^\beta(t)>$ of eq. (4.11) to be

$$\begin{aligned}
<\hat{S}_i^x(0)\hat{S}_j^x(t)> &= \frac{S}{2N}\sum_q \left[\exp\left\{-i\left[\mathbf{q}\cdot(\mathbf{R}_i-\mathbf{R}_j)-\omega(\mathbf{q})t\right]\right\}<n_q+1>\right. \\
&\quad \left. + \exp\left\{i\left[\mathbf{q}\cdot(\mathbf{R}_i-\mathbf{R}_j)-\omega(\mathbf{q})t\right]\right\}<n_q>\right], \\
<\hat{S}_i^y(0)\hat{S}_j^y(t)> &= <\hat{S}_i^x(0)\hat{S}_j^x(t)>, \\
<\hat{S}_i^z(0)\hat{S}_j^z(t)> &= S^2 - \frac{2S}{N}\sum_q <n_q>,
\end{aligned} \tag{6.20}$$

where $<n_q>$ is the Bose-Einstein occupation number:

$$<n_q> = \left[\exp\left\{\frac{\hbar\omega(q)}{k_BT}\right\}-1\right]^{-1}. \tag{6.21}$$

For the calculation of the neutron cross-section for spin-wave scattering we insert eq. (6.20) into the "master formula" (eqs. 4.6 and 4.11). We can drop the term $\alpha=\beta=z$ which is time-independent, i.e., it describes the elastic magnetic scattering. Moreover, since $<\hat{S}_i^x(0)\hat{S}_j^y(t)>=-<\hat{S}_i^y(0)\hat{S}_j^x(t)>$, we are left with the terms $\alpha=\beta=x$ and $\alpha=\beta=y$:

$$\frac{d^2\sigma}{d\Omega d\omega} = (\gamma r_o)^2 \frac{S}{4\pi\hbar}\frac{k'}{k} F^2(\mathbf{Q})\exp\{-2W(\mathbf{Q})\}\left(1+\frac{Q_z^2}{Q^2}\right)\sum_{i,j}\exp\left\{i\mathbf{Q}\cdot(\mathbf{R}_i-\mathbf{R}_j)\right\}$$

$$\int_{-\infty}^{+\infty}\sum_{\mathbf{q}}\left[\exp\left\{-i\left[\mathbf{q}\cdot(\mathbf{R}_i-\mathbf{R}_j)-\omega(\mathbf{q})t\right]\right\}<n_{\mathbf{q}}+1> \right. \tag{6.22}$$

$$\left. + \exp\left\{i\left[\mathbf{q}\cdot(\mathbf{R}_i-\mathbf{R}_j)-\omega(\mathbf{q})t\right]\right\}<n_{\mathbf{q}}>\right]\exp\{-i\omega t\}\ dt\ .$$

Using the relation for the lattice sum,

$$\sum_{i>j}\exp\left\{i\mathbf{Q}\cdot(\mathbf{R}_i-\mathbf{R}_j)\right\} = \frac{(2\pi)^3}{v_o}\sum_{\tau}\delta(\mathbf{Q}-\tau)\ , \tag{6.23}$$

where v_o is the volume of the unit cell, and the integral representation of the δ-function (see eq. 4.10) we arrive at the final formula:

$$\frac{d^2\sigma}{d\Omega d\omega} = (\gamma r_o)^2\ \frac{(2\pi)^3 S}{2v_o}\ \frac{k'}{k}\ F^2(\mathbf{Q})\ \exp\{-2W(\mathbf{Q})\}\left(1+\frac{Q_z^2}{Q^2}\right)$$

$$\sum_{\tau,\mathbf{q}}\left[<n_{\mathbf{q}}+1>\ \delta(\mathbf{Q}-\mathbf{q}-\tau)\ \delta\{\hbar\omega(\mathbf{q})-\hbar\omega\}\right. \tag{6.24}$$

$$\left. + <n_{\mathbf{q}}>\ \delta(\mathbf{Q}+\mathbf{q}-\tau)\ \delta\{\hbar\omega(\mathbf{q})+\hbar\omega\}\right]\ .$$

The cross section (6.24) is the sum of two terms, the first corresponding to the creation and the second to the annihilation of a spin wave. We recognize that the two δ-functions in the cross section describe the momentum and energy conservation of the neutron scattering process according to eqs. (3.1) and (3.2), respectively.

Let us consider as an example the spin waves in the antiferromagnet $YBa_2Cu_3O_{6.15}$, the parent compound of the T_c=90 K superconductor $YBa_2Cu_3O_7$. In this structure the spin waves propagate within two coupled CuO_2 planes. The Heisenberg Hamiltonian reads

$$\hat{H} = \sum_{ij} J_{\parallel}\ \hat{S}_i\cdot\hat{S}_j + \sum_{ik} J_{\perp}\ \hat{S}_i\cdot\hat{S}_k\ , \tag{6.25}$$

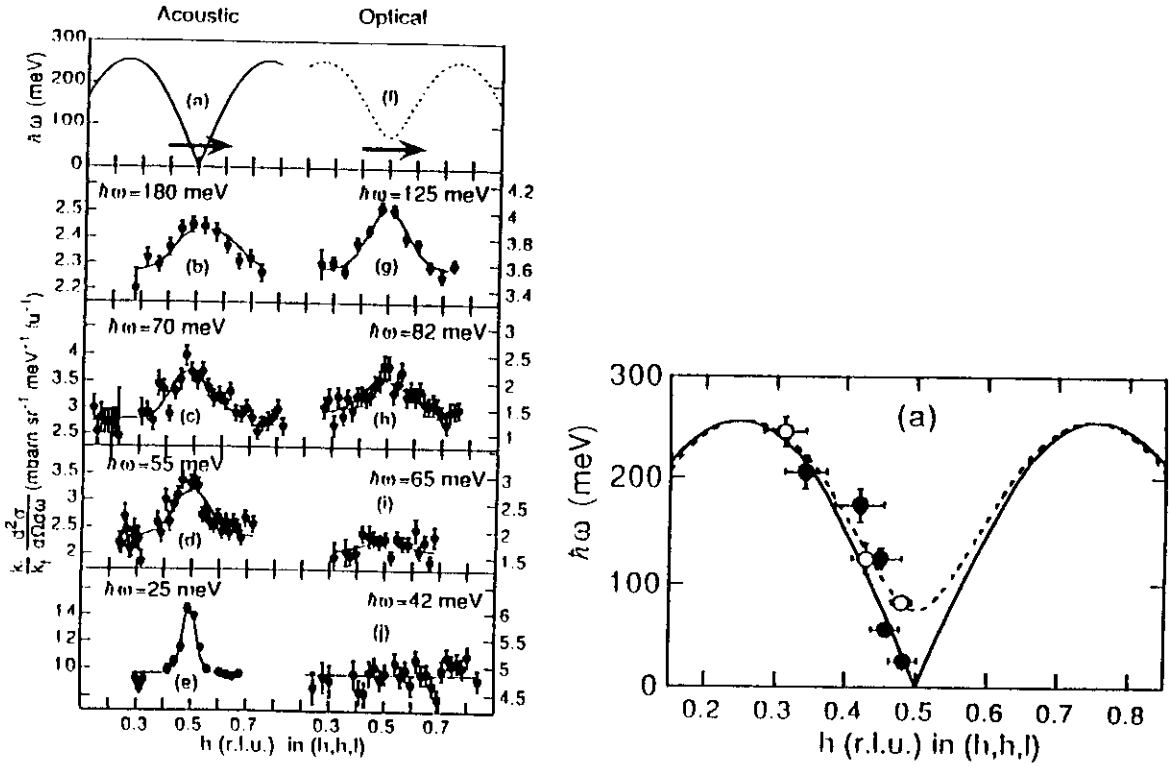

Fig. 6.3: Left hand side: Energy spectra of neutrons scattered from $YBa_2Cu_3O_{6.15}$ [Hayden et al., Phys. Rev. B **54**, R6905 (1996)]. Right hand side: Resulting spin-wave dispersion.

where the first term denotes the intraplanar, the second term the interplanar exchange coupling between nearest-neighbour Cu spins. We have two spin-wave dispersion branches, since there are two Cu ions per unit cell:

$$\hbar\omega(\vec{Q}) = 2J_{\parallel}[1 - \gamma^2(\vec{Q}) + \frac{J_{\perp}}{2J_{\parallel}}\{1 \pm \gamma(\vec{Q})\}]^{1/2} ,$$
$$\text{with } \gamma(\vec{Q}) = \tfrac{1}{2}[\cos(aQ_x) + \cos(aQ_y)] \ . \qquad (6.26)$$

Herein the the + sign denotes the acoustic, the – sign the optic spin-wave branch. a=3.855 Å is the lattice parameter along the x and y axes. For instance, at the antiferromagnetic zone center $\vec{Q} = (2\pi/a,\ 2\pi/a,\ Q_z)$ the optic spin-wave branch exhibits a gap of energy $\hbar\omega_g = 2\sqrt{J_{\parallel}J_{\perp}}$. By applying eq. (6.22) we can differentiate between acoustic and optic spin waves (see Fig. 6.3):

$$\left(\frac{d^2\sigma}{d\Omega d\omega}\right)_{ac} \approx \cos^2\left(\tfrac{1}{2}\Delta z Q_z\right) ; \quad \left(\frac{d^2\sigma}{d\Omega d\omega}\right)_{op} \approx \sin^2\left(\tfrac{1}{2}\Delta z Q_z\right) . \tag{6.27}$$

Δz=3.2 Å is the distance between the two CuO_2 planes. Obviously we can only observe acoustic spin waves for $Q_z c/2\pi$=1.8, 5.5, ..., and optic spin waves for $Q_z c/2\pi$=3.7, 7.3, ... (c=11.8 Å is the lattice parameter along the z axis).

7. References

[1] G.S. Bauer, in *Neutron Scattering*, ed. by A. Furrer, PSI-Proceedings No. 93-01, ISSN 1019-6447 (Paul Scherrer Institute, Villigen, 1993), p. 331.

[2] B.N. Brockhouse, *Can. J. Phys.* **33**, 889 (1955).

[3] O. Halpern and M.H. Johnson, *Phys. Rev.* **55**, 898 (1939).

[4] G.L. Squires, *Thermal Neutron Scattering* (Dover Publications, Mineola, New York, 1996), p. 129.

[5] S.W. Lovesey, *Theory of Neutron Scattering from Condensed Matter*, Vol. 2, *International Series of Monographs on Physics 72* (Oxford Science Publishers, Oxford, 1987), p. 1.

[6] D.F. Johnston, *Proc. Phys. Soc.* **88**, 37 (1966).

[7] L. van Hove, *Phys. Rev.* **93**, 268 (1954).

[8] A.R. Mackintosh, in *The Neutron and its Applications*, Conference Series No. 64 (The Institute of Physics, Bristol and London, 1983), p. 199.

[9] A. Abrikosov, *Soviet Physics JETP* **5**, 1174 (1957).

[10] E.M. Forgan, in *Neutron Scattering in Layered Copper-Oxide Superconductors*, ed. A. Furrer (Kluwer Academic Publishers, Dordrecht/Boston/London, 1998), p. 375.

[11] T. Holstein and H. Primakoff, *Phys. Rev.* **58**, 1098 (1940).